ACS APPLIED MATERIALS & INTERFACES

Research Article

www.acsami.org

Ultratrace Detection of Nitroaromatics: Picric Acid Responsive Aggregation/Disaggregation of Self-Assembled *p*-Terphenylbenzimidazolium-Based Molecular Baskets

Sana Sandhu,[†] Rahul Kumar,[†] Prabhpreet Singh,*[,†] Aman Mahajan,[‡] Manmeet Kaur,[§] and Subodh Kumar*[,†]

[†]Department of Chemistry, UGC Center for Advanced Studies and [‡]Department of Physics, Center for Material Science Research, Guru Nanak Dev University, Amritsar, Punjab 143005, India

[§]Bhabha Atomic Research Center, Mumbai, India

Supporting Information

ABSTRACT: 1-(*p*-Terphenyl)-benzimidazolium (TRIPOD-TP) molecules undergo self-assembly to form rodlike structures in aqueous medium, as shown by field-emission scanning electron microscopy, transmission electron microscopy, and dynamic light scattering studies. Upon gradual addition of picric acid (PA), these aggregates undergo an aggregation/disaggregation process to complex morphological structures (10^{-12}–10^{-10} M PA) and spherical aggregates (10^{-9}–10^{-8} M PA). These spherical aggregates undergo further dissolution to well-dispersed spheres between 10^{-7}–10^{-6} M PA. During fluorescence studies, these aggregates demonstrate superamplified fluorescence quenching (>97%) in the presence of 10^{-5} to 0.2 equiv of the probe concentration, an unprecedented process with PA. The lowest detection limits by solution of TRIPOD-TP are 5×10^{-13} PA, 50×10^{-12} M 2,4-dinitrophenol, 200×10^{-12} M 2,4,6-trinitrotoluene, and 1 nM 1-chloro-2,4-dinitrobenzene. Paper strips dipped in the solution of TRIPOD-TP demonstrate quantitative fluorescence quenching between 10^{-17} and 10^{-6} M PA using front-surface steady state studies and can measure as low as 2.29×10^{-20} g/cm^2 PA.

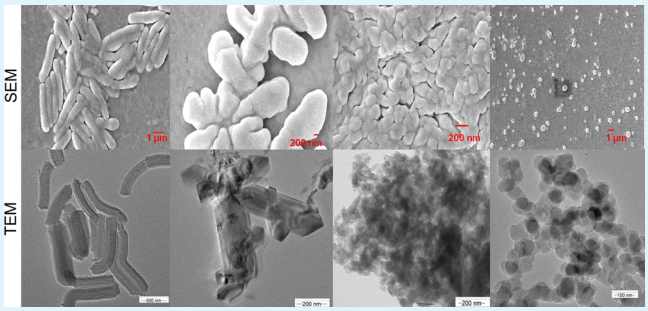

KEYWORDS: *self-assembly, aggregation, disaggregation, nitro-aromatic explosives, amplified fluorescence quenching, vapor detection*

INTRODUCTION

Nitro aromatic compounds (NACs) such as 2,4,6-trinitrotoluene (TNT), 2,4-dinitrotoluene (DNT), 1,3,5-trinitro-perhydro-1,3,5-triazine (RDX), and picric acid (PA), the main ingredients in explosives, have attracted increasing attention for protection against threats of terrorism at entrance portals and other domestic locations, such as buses, trains, buildings, and so forth. These NACs are also continuously being released into the environment during their commercial production or leaching from military waste sites, mining activity, and space experiments. Degradation of these NACs leads to the generation of reactive nitrogen oxide species, which readily react with biological macromolecules and cause the formation of potent genotoxic and mutagenic metabolites.[1−6] Thus, being able to detect NACs at ultra low levels has become an urgent issue in the interest of both national security and environmental protection.[7−15]

The analysis of fluorescence signals for the detection of NACs has emerged as a prominent technique by virtue of its high detection sensitivity, selectivity, and applicability in both solution and solid phase.[16] Fluorescent-conjugated polymers[17−26] with excellent molar absorptivity, high quantum yields, and amplified sensory responses, have been found to be advantageous relative to small fluorescent molecules. Swager et al. have a number of reports[27−32] describing trace detection of TNT and its commercialized product FidoXT, which has been applied in war zones.

In another approach, several fluorescent nanofibers[33−43] obtained by self-assembly of simple molecular systems have been reported as sensing materials for the detection of nitro aromatic explosives. Effective π–π stacking between these molecules provides ordered molecular organization and enables long-range exciton migration and their quick annihilation by the explosive quenchers.

However, research on NACs is primarily directed toward the detection of TNT and less attention has been paid to picric acid (PA) even though its explosive power is superior to that of TNT.[44] Thus, it is of extreme importance to develop self-assembled molecular probes that can undergo aggregation/disaggregation processes in the presence of picric acid to the single molecule stage to thus provide a level of ultratrace detection of picric acid. Further, probes that can detect PA at

Received: March 5, 2015
Accepted: April 27, 2015
Published: April 27, 2015

DOI: 10.1021/acsami.5b01970
ACS Appl. Mater. Interfaces 2015, 7, 10491−10500

less than nano or even pico molar concentrations from solutions or vapors are essential for practical applications in the detection of trace amounts of PA.

In continuation of our work[45] designing molecular probes for NACs, in this study, we have designed and synthesized a new 1-(*p*-terphenyl)-benzimidazolium-based probe (TRIPOD-TP), which in water/DMSO (2%) undergoes aggregation/disaggregation-modulated detection of picric acid (PA). Field-emission scanning electron microscopy (SEM), transmission electron microscopy (TEM), and dynamic light scattering (DLS) studies demonstrate the formation of self-assembled rodlike structures. In the presence of increasing amounts of PA from 10^{-12} to 10^{-6} M, these aggregates undergo a complex aggregation/disaggregation process before their dissolution to well-dispersed spheres. The blue emission of these aggregates undergoes superamplified fluorescence quenching (>97%) in the presence of 0.2 equiv of TRIPOD-TP concentration, in both solution and solid state. TRIPOD-TP can detect 5×10^{-13} M (500 *f*M) PA in solution phase and as low as 10 μL of 10^{-17} M (i.e., 2.29×10^{-20} g/cm^2) PA using TRIPOD-TP-coated paper strips. 2,4-Dinitrophenol (DNP), 2,4,6-trinitrotoluene (TNT), and 1-chloro-2,4-dinitrobenzene (ClDNB) can be detected but at much higher concentrations. Other NACs do not show any response even at equivalent amounts.

RESULTS AND DISCUSSION

TRIPOD-TP was synthesized in 90% yield by heating a 3:1 mixture of compounds **1** and **2** in acetonitrile at 90 °C under N_2 (Scheme 1). The structure of TRIPOD-TP was confirmed

Scheme 1. Synthesis of TRIPOD-TP

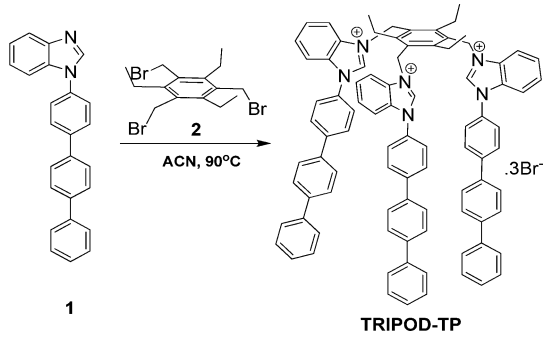

by spectroscopic techniques using ^{1}H NMR, ^{13}C NMR, and HRMS (see Supporting Information (SI) for synthesis details and structural characterization).

To find the appropriate solvent medium for studying interactions of TRIPOD-TP with PA, the fluorescence of TRIPOD-TP in DMSO and DMSO/water mixtures containing varying amounts of water was determined. The plot of I_o/I shows a regular but small increase in value upon increasing the the ratio of water up to 80%, and then the I_o/I ratio increases sharply, suggesting aggregation of TRIPOD-TP in >90% aqueous medium (Figure 1a, Figure S1 in the SI). The fluorescence spectrum of TRIPOD-TP in DMSO and aqueous media with up to 90% water ratio gave emission maxima between 450−465 nm, but upon increasing the amount of water to ≥95%, the emission maxima was blue-shifted to between 402 and 410 nm. This further confirms the aggregation of TRIPOD-TP molecules at water ratios ≥95%.

To further ascertain the formation of aggregates, DLS analysis (Figure 1b) of these solutions was recorded. In

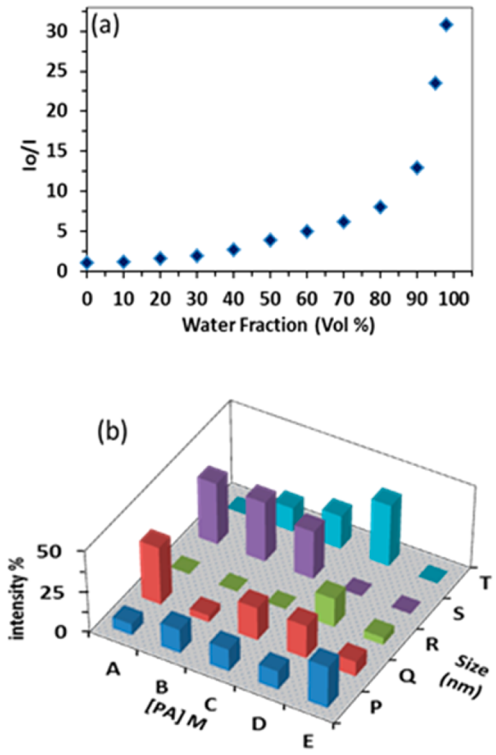

Figure 1. (a) The effect of the water ratio on I_o/I of the solutions of TRIPOD-TP (5 μM). (b) Distribution of different sized particles in a polydispersed solution of TRIPOD-TP (10 μM, 98:2 water/DMSO) upon the gradual addition of picric acid aliquots. P, 40−100 nm; Q, 100−200 nm; R, 220−396 nm; S, 531−712 nm; T, >800 nm. A, TRIPOD-TP (10 μM); B, A + 10^{-10} M PA; C, A + 10^{-9} M PA; D, A + 10^{-8} M PA; E, A + 10^{-7} M PA.

solutions containing <90% water, light scattering was not observed. Upon increasing the amount of water to 95 or 98%, polydispersity of particles between 50 and 900 nm in size with a *Z*-average of 785 nm was observed. Thus, all of the studies were performed in a 98:2 water/DMSO mixture as the solvent. The DLS experiment of the TRIPOD-TP solution showed the formation of aggregates only between 100−200 nm and 530−712 nm in size. Upon the addition of picric acid (10^{-10} M), the intensity of the aggregates between 100 and 200 nm in size was drastically decreased and aggregates with a size of >800 nm made a significant (14.3%) contribution. Upon further increasing the concentration of picric acid to 10^{-9} and 10^{-8} M, the contribution of aggregates with >800 nm in size was further increased to 20 and 37%, respectively. However, upon increasing the concentration of PA to 10^{-7} M, all of these aggregates dissolved to a size of <200 nm (Figure 1b). Therefore, self-assembled aggregates of TRIPOD-TP in 98:2 water/DMSO undergo aggregation/disaggregation processes upon the gradual addition of PA. The formation of these aggregates and their aggregation/disaggregation processes in the presence of varied amounts of PA has been substantiated by field-emission scanning (FESEM) and transmission electron (TEM) microscopic techniques.

Field-Emission Scanning Electron and Transmission Electron Microscopic Studies. The FESEM image of a drop-cast thin-film of the solution of TRIPOD-TP demonstrated self-assembly of TRIPOD-TP molecules into rodlike structures (Figure 2a, b). Figure 2b shows the high porosity in these rods, which can capture small NAC molecules through electrostatic

DOI: 10.1021/acsami.5b01970
ACS Appl. Mater. Interfaces 2015, 7, 10491−10500

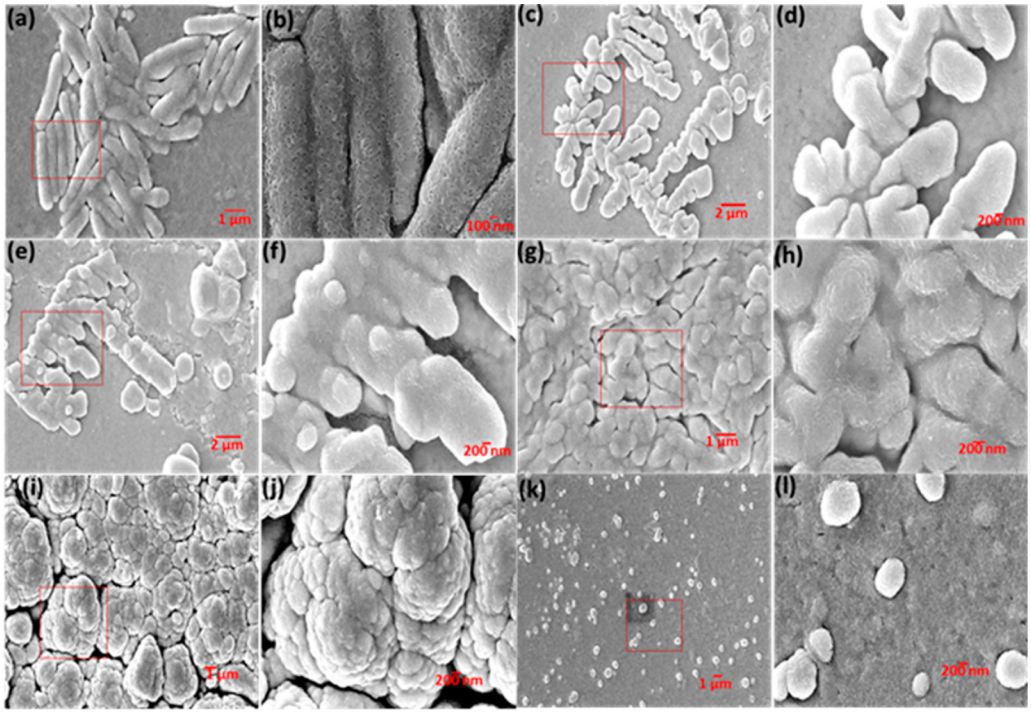

Figure 2. Morphological changes in TRIPOD-TP upon the addition of various amounts of picric acid. (a) [PA] = 0 M; (b) magnified view of selected area in (a); (c) [PA] = 10^{-12} M; (d) magnified view of selected area in (c); (e) [PA] = 5×10^{-11} M; (f) magnified view of selected area in (e); (g) [PA] = 10^{-9} M; (h) magnified view of selected area in (g); (i) [PA] = 5×10^{-8} M; (j) magnified view of selected area in (i); (k) [PA] = 2×10^{-7} M; (l) magnified view of selected area in (k).

interactions and/or hydrophobic $\pi-\pi$ interactions with respective benzimidazolium and terphenyl units. TEM images of TRIPOD-TP (Figure 3a, b) also showed the formation of

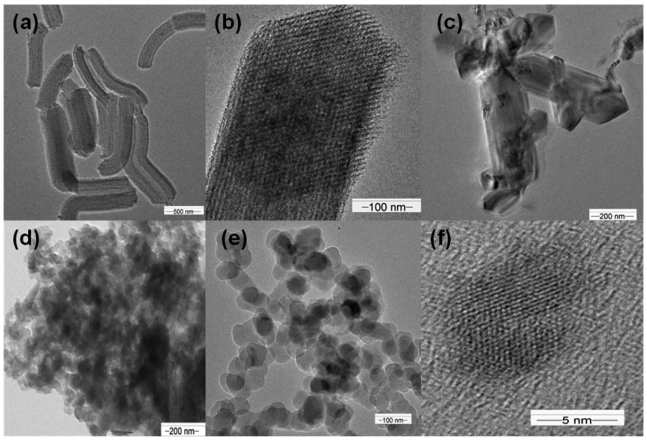

Figure 3. TEM images of (a, b) TRIPOD-TP (5 μM); (c) TRIPOD-TP (5 μM) + PA (10^{-12} M), (d) TRIPOD-TP (5 μM) + PA (10^{-9} M); (e, f) TRIPOD-TP (5 μM) + PA (2×10^{-7} M) in 98:2 H_2O/DMSO.

similar rodlike morphology. To substantiate the amorphous or crystalline phases of these rods, selected area electron diffraction (SAED) of these rods was performed inside the transmission electron microscope. The absence of any diffraction spots in SAED of these rods (Figure S2, SI) clearly demonstrated their amorphous nature. X-ray diffraction analysis of the solid TRIPOD-TP precipitated from a DMSO/water (1:1) mixture showed a broad peak (Figure S3, SI), further supporting the amorphous nature of the material. The increased resolution of these rods in HR TEM (Figure 3b) showed their formation by self-assembly of threads with ~1.5 nm diameter and 800−900 nm length. These threads could be further resolved into small dots in HR TEM. The energy minimized structure (Figure S4, SI) of TRIPOD-TP was calculated using density functional theory with the B3LYP/6-31G basis set. The length and breadth of the TRIPOD-TP was found to be ~2.0 and 1.5 nm, respectively. By considering the length of the TRIPOD-TP molecule, it seems that each thread is formed by linear aggregation of TRIPOD-TP molecules where each dot represents one phenyl ring. These threads are separated by ~2.5 nm, representing the width (1.5 nm) of the TRIPOD-TP molecule. Significantly, an earlier reported 1-(4-biphenyl)benzimidazolium-based tripodal system formed a well-organized basketlike structure[45] but did not undergo aggregation under similar conditions. As the hydrophobic *p*-terphenyl units are well-known for causing aggregation,[54−58] aggregation of the TRIPOD-TP molecules in the present studies could be attributed to the presence of *p*-terphenyl moieties.

The drop-cast thin film of TRIPOD-TP solution possessing 10^{-12} M PA showed the beginning of the morphological change in rodlike structures (Figure 2c, d), where both aggregation and disaggregation of these rods was apparent. This beginning of morphological changes in TRIPOD-TP was also evident in the TEM image (Figure 3c). FESEM images of thin films containing 5×10^{-11} M PA in TRIPOD-TP (Figure 2e, f) demonstrated the initial formation of spherical aggregates along with rodlike structures. The film obtained from TRIPOD-TP containing 10^{-9} M PA (Figure 2g, h) showed almost complete conversion to spherical aggregates, and this process was completed when the concentration of PA was increased to 5×10^{-8} M (Figure 2i, j), and spherical aggregates with diameters

DOI: 10.1021/acsami.5b01970
ACS Appl. Mater. Interfaces 2015, 7, 10491−10500

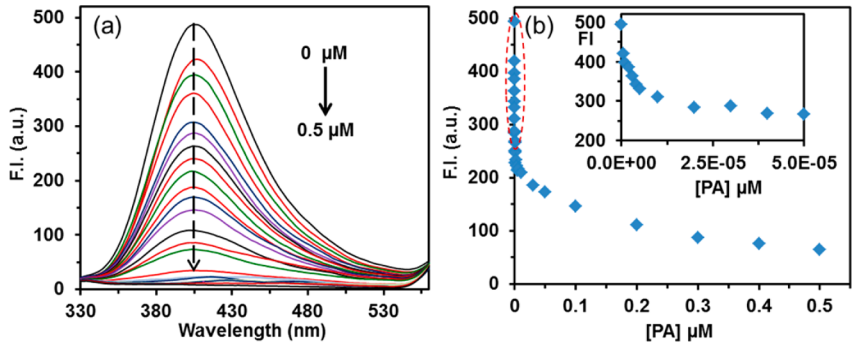

Figure 4. (a) The gradual decrease in fluorescence intensity (FI) upon addition of aliquots of PA to the solution of TRIPOD-TP (5 μM, 98:2 H_2O/DMSO), λ_{ex} = 290 nm, and (b) plot of FI vs [PA]. Inset: plot of FI vs [PA] showing the sensitivity of the TRIPOD-TP probe toward PA.

between 200 and 600 nm were formed. The formation of these spherical aggregates was also confirmed by TEM imaging (Figure 3d).

Upon further increasing the concentration of PA to 2×10^{-7} M in TRIPOD-TP (5 μM) solution, the FESEM image of the thin-films showed a drastic decrease in the concentration of spheres (Figure 2k and l). The TEM image of a similar film obtained on a copper grid (Figure 3e, f) also confirmed the formation of spherical aggregates with 50−60 nm diameter, which could undergo further aggregation to form larger sized aggregates. Recording of SAED and XRD powder data on these spherical aggregates points to their amorphous nature (Figures S5 and S6, SI). Upon further increasing the concentration of PA to 5×10^{-6} M in TRIPOD-TP (5 μM) solution, aggregate formation was not observed, which was in agreement with no-scattering of light in the DLS studies. This clearly shows that at 1 equiv of PA, the interaction of PA with TRIPOD-TP is purely at the molecular level and is in consonance with almost complete quenching (>97%) of the fluorescence intensity of TRIPOD-TP in the solution phase (Figure 4). Therefore, the overall mechanism of aggregation/disaggregation of TRIPOD-TP can be understood in the following manner. PA enters into the rodlike morphology of TRIPOD-TP and leads to breaking of the aggregates. This results in further reorganization of the newly formed aggregates, leading to complex morphological structures. After the addition of 10^{-7} to 10^{-6} M PA, dissolution of these aggregates to well-dispersed spheres occurs, which are finally dissolved to make a homogeneous solution.

Moreover, the FESEM images of thin films of TRIPOD-TP obtained after the addition of a 1 nM concentration of TNT and 1-chloro-2,4-dinitrobenzene (ClDNB) apparently retained the rodlike morphology of the thin film of pure TRIPOD-TP. Therefore, the rodlike morphology of TRIPOD-TP is quite stable to TNT and ClDNB at concentrations <1 nM. These results are in consonance with the poor fluorescence response of TRIPOD-TP solutions toward TNT and ClDNB at <1 nM concentrations, as discussed in the next section. Upon increasing the concentration of TNT to 10^{-6} M, the corresponding thin film showed the formation of 140−170 nm sized spheres (Figure 5a). In the case of 10^{-6} M ClDNB, the formation of a mixture of 20−40 nm particles and platelet-like structures was observed (Figure 5b). However, the thin film of TRIPOD-TP obtained after the addition of a 10^{-10} M concentration of 2,4-DNP showed rods as well as aggregated spheres, which were changed to densely populated spheres of ~30 nm size at 10^{-8} M concentration of 2,4-DNP (Figure 5c, d). Therefore, TRIPOD-TP underwent morphological changes

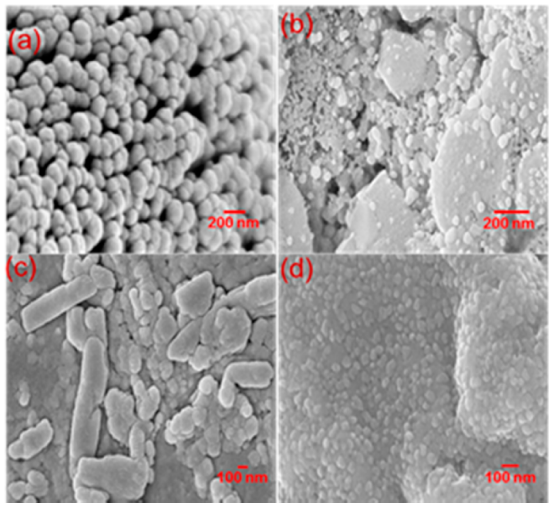

Figure 5. Morphological changes in TRIPOD-TP upon the addition of various amounts of (a) [TNT] = 10^{-6} M, (b) [ClDNB] = 10^{-6} M, (c) [2,4-DNP] = 10^{-10} M, and (d) [2,4-DNP] = 10^{-8} M.

with respect to the amount of various NACs in the order PA > 2,4-DNP > TNT ~ ClDNB.

UV−Vis and Fluorescence Spectroscopy. We hypothesized that TRIPOD-TP, due to its rodlike porous structure, could facilitate the binding process with PA and would also result in changes of its optical properties. The UV−vis absorption spectrum of TRIPOD-TP (5 μM, 98:2 water/DMSO) exhibited an absorption band at 270 nm (ϵ = 65000). Upon excitation at 290 nm, the solution of TRIPOD-TP (5 μM) gave λ_{em} centered at 402 nm (Φ = 0.05). The UV−vis absorption spectrum of TRIPOD-TP did not show any significant change in its spectrum upon the addition of 10^{-10} M concentration of various (nitro)aromatic compounds, including phenol, 2-nitrophenol (2-NP), 4-nitrophenol (4-NP), 2,4-dinitrophenol (2,4-DNP), picric acid (PA), 4-hydroxybiphenyl (4-OHBP), 2-nitrotoluene (2-NT), 2,4-dinitrotoluene (2,4-DNT), dinitrobenzene (DNB), 2-chloronitrobenzene (2-ClNB), 2,4,6-trinitrotoluene (TNT), 3-chloronitrobenzene (3-ClNB), 4-chloro-nitrobenzene (4-ClNB), 1-chloro-2,4-dinitrobenzene (ClDNB), 2-nitroaniline (2-NA), and 2,4-dinitroaniline (2,4-DNA) (Figure 6a). Therefore, the formation of a charge-transfer complex between TRIPOD-TP and nitro-aromatic compounds, especially picric acid, is ruled out. However, the emission spectrum of TRIPOD-TP, upon the addition of 10^{-10} M PA, resulted in 40% quenching of the fluorescence intensity, whereas the addition of other closely

DOI: 10.1021/acsami.5b01970
ACS Appl. Mater. Interfaces 2015, 7, 10491−10500

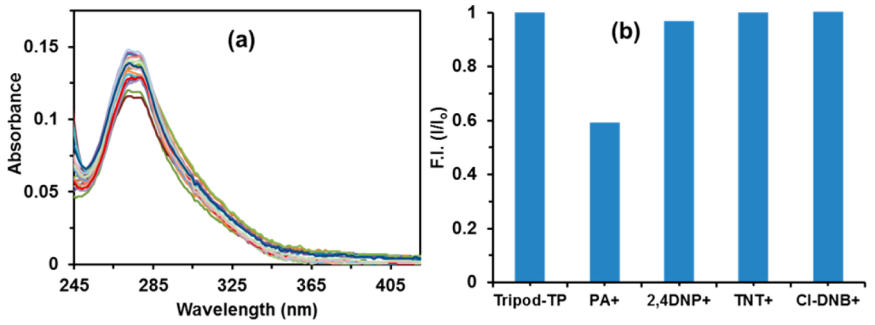

Figure 6. (a) UV−vis spectrum of TRIPOD-TP (5 μM, 98:2 H_2O/DMSO) upon the addition of various NACs. (b) Effect of various NACs (10^{-10} M) on the emission intensity of TRIPOD-TP at 402 nm in 98:2 water/DMSO. The (+) indicates the NAC + TRIPOD-TP.

related NACs, such as 2,4-DNP, TNT, and ClDNB (10^{-10} M each) caused <1% change in the fluorescence intensity of TRIPOD-TP (Figure 6b). The addition of 0.1 equiv (0.5 μM) of the NACs PA, 2,4-DNP, TNT, and ClDNB resulted in 88, 70, 39, 20 percent quenching, respectively. The other NACs had a minimal effect on the fluorescence intensity of the TRIPOD-TP solution. Therefore, at sub-nanomolar concentrations of NACs, TRIPOD-TP is highly selective and sensitive toward PA.

Upon the gradual addition of aliquots of PA to the solution of TRIPOD-TP (5 μM, 98:2 water/DMSO), the fluorescence intensity at 402 nm was gradually quenched up to the addition of 0.1 equiv of PA, and upon further addition of PA, no significant change in fluorescence intensity was observed (Figure 4). The plot of fluorescence intensity vs [PA] is nonlinear, and fluorescence intensity decreases exponentially with an increase in the concentration of PA. The present system is unique, which shows amplified quenching at <0.1 equiv of PA, and its sensitivity outperforms previously reported PA chemosensors. In the literature,[46−50] superamplified quenching has been observed only at very high concentrations of NACs.

The plot of I/I_o vs log[PA] demonstrates three steps of linear change between 5×10^{-13} and 5×10^{-11} M, 5×10^{-11} and 5×10^{-8} M, and 5×10^{-8} and 1×10^{-6} M concentrations of PA (Figure 7). Consequently, Stern−Volmer constants (K_{SV}) have been determined for these three different ranges of concentrations using the exponential equation ($I/I_o = Ae^{k[Q]} + B$),[43,50−52] and were found to be 1.20×10^{11} M^{-1}, 1.10×10^{8} M^{-1}, and 4.8×10^{5} M^{-1}, respectively. The lowest limit of detection for PA was 5×10^{-13} M.[53]

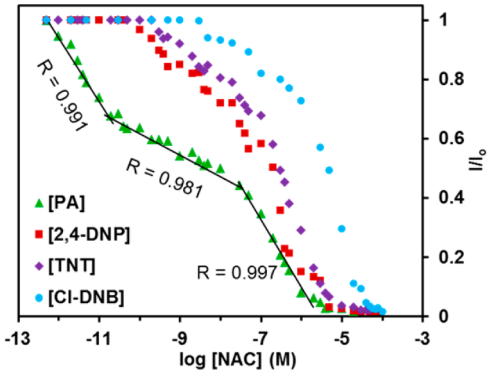

Figure 7. Plot of fluorescence intensity (I/I_o) of TRIPOD-TP (5 μM, 98:2 H_2O/DMSO vs log[NAC]).

To rationalize the interaction of TRIPOD-TP with PA, we recorded the ^{1}H NMR spectrum of TRIPOD-TP before and after the addition of PA in DMSO-d_6/water (7:3) at a concentration of 5 mM. It could not be recorded in water (with 2% DMSO), the solvent of all of the photophysical and morphological studies, due to its poor solubility in this medium at such high concentration. In the ^{1}H NMR spectrum of the solution of a 1:1 mixture of TRIPOD-TP and PA, the upfield shift of the 2H singlet of PA to δ 8.32 from 8.62 (in the ^{1}H NMR spectrum of PA) points to the encapsulation of PA in the cavity of TRIPOD-TP (Figure S7, SI).

To further explore the utility of TRIPOD-TP for the detection of PA vapors, we fabricated the thin film on a glass plate by the drop-cast technique [20 μL of TRIPOD-TP (10 μM)]. The fluorescence intensity of the thin film was recorded as it was exposed to the saturated vapors of PA at regular time intervals. The fluorescence intensity of the thin film started decreasing as soon as it came in contact with PA vapors, and the initial fluorescence emission intensity significantly decreased to 25% after exposure of the thin film for 120 s. Upon continuous exposure to PA vapors, maximum fluorescence quenching was observed within 360 s (Figure 8). The thin film

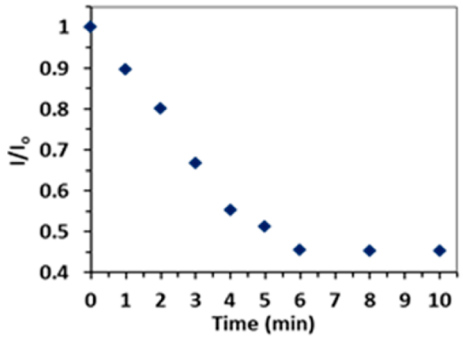

Figure 8. Variation in fluorescence intensity of a drop-cast thin film of TRIPOD-TP upon exposure to PA vapors.

exposed to saturated vapors of PA for 600 s did not revive fluorescence intensity upon washing with water. Therefore, binding of PA on thin films is irreversible. The nonvariation in the lifetime of thin films in the presence of PA vapors supports a static mechanism.

Similarly, the addition of 0.1 equiv of other NACs, including 2,4-DNP, TNT, and ClDNB, to the solution of TRIPOD-TP demonstrated 70, 39, and 20% quenching of fluorescence intensity, respectively, and exhibited an amplified quenching effect at 0.1 equiv of TRIPOD-TP. In all of these cases, the plot

DOI: 10.1021/acsami.5b01970
ACS Appl. Mater. Interfaces 2015, 7, 10491−10500

of fluorescence intensity vs [NAC] shows a nonlinear change in the fluorescence quenching of the solution of TRIPOD-TP (Figure 9a–c). The plot of I/I_o vs log [NAC] demonstrates

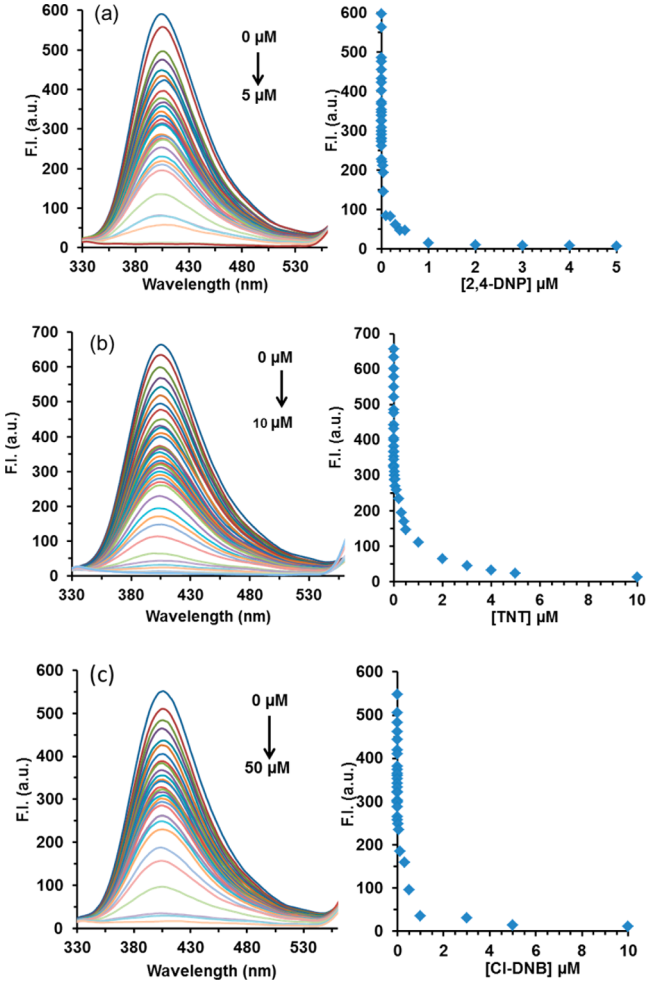

Figure 9. Fluorometric titration of TRIPOD-TP (5 μM, 98:2 H_2O/DMSO) with incremental additions of (a) 2,4-DNP, (b) TNT, and (c) ClDNB; λ_{ex} = 290 nm.

more than one segment for the linear change in I/I_o with respect to log [NAC] (Figure 7). The K_{SV} values for these NACs have been determined using the exponential equation $(I/I_o = Ae^{k[Q]} + B)$[43,50−52] and are given in Table 1. The minimum detection limits[53] for 2,4-DNP, TNT, and ClDNB were 50 × 10^{-12} M, 200 × 10^{-12} M, and 1 nM, respectively. These detection limits are at concentrations ≥100 times higher in comparison to the lowest detection limit observed for PA. Therefore, the sensitivity of TRIPOD-TP is on the order of PA > 2,4-DNP > TNT > ClDNB.

In addition to electrostatic interactions between the picrate ion and the benzimidazolium moieties of TRIPOD-TP, the efficiency of electron transfer from the HOMO of NACs to the LUMO of TRIPOD-TP may also contribute to the selectivity of TRIPOD-TP toward PA. To rationalize the contribution of electron transfer in selective fluorescence quenching, the structures of TRIPOD-TP and NACs were optimized, and the energies of their HOMOs and LUMOs were calculated. The HOMO of picrate anion lies at an energy ∼35.8 kcal/mol (Figure S8, SI) above the LUMO of TRIPOD-TP. Therefore, the electron transfer from the HOMO of picrate anion to the LUMO of TRIPOD-TP results in fluorescence quenching. In the case of 2,4-DNP, although its HOMO lies above the LUMO of TRIPOD-TP, a larger energy difference (∼56 kcal/mol) between the HOMO of 2,4-DNP anion and LUMO of TRIPOD-TP results in significantly lower efficiency of electron transfer and thus efficiency of fluorescence quenching. Theoretical calculations also revealed that the HOMOs of TNT and ClDNB are lower in energy than the LUMO of TRIPOD-TP and are responsible for the poor sensitivity of TRIPOD-TP toward TNT and ClDNB. Therefore, TRIPOD-TP undergoes more efficient fluorescence quenching with PA than with 2,4-DNP, TNT, or ClDNB.

Contact Mode Methods for the Detection of Trace Amounts of PA. Finally, we investigated the applicability of TRIPOD-TP in both qualitative and quantitative detection of picric acid using the contact mode method. For this, we carried out experiments on paper strips coated with TRIPOD-TP, which were then visualized under 365 nm UV light. We observed that the addition of 10 μL of 10^{-17} M PA causes visible quenching of the fluorescence intensity on the paper strip (Figure 10B). Complete quenching of fluorescence intensity was observed with 10^{-9} M PA (Figure 10E), and the addition of higher concentrations of PA caused a black color area to develop on the paper strip. Figure 10A shows no quenching of fluorescence with only water. Therefore, the minimum amount of PA detectable is 2.29 × 10^{-20} g/cm^2

Table 1. K_{SV} Values for the Interaction of TRIPOD-TP with NACs by Applying Exponential Equation $I/I_o = Ae^{Ksv[Q]} + B$ from Nonlinear Curve-Fitting Using Origin Software[a]

NAC	conc. range (M)	K_{SV} (M^{-1})	R value	LOD	NAC max[x]
PA	5 × 10^{-13}–5 × 10^{-11}	1.20 × 10^{11}	0.99	0.5 pM	0.1
	5 × 10^{-11}–5 × 10^{-8}	1.10 × 10^{8}	0.98	0.5 pM	
	5 × 10^{-8}–1 × 10^{-6}	4.78 × 10^{5}	0.99	0.5 pM	
2,4-DNP	4 × 10^{-12}–4 × 10^{-9}	4.52 × 10^{9}	0.93	50 pM	1
	2 × 10^{-8}–1 × 10^{-6}	1.83 × 10^{6}	0.99	50 pM	
	2 × 10^{-8}–1 × 10^{-5}	2.73 × 10^{5}	0.99	50 pM	
TNT	5 × 10^{-11}–4 × 10^{-8}	2.29 × 10^{8}	0.97	200 pM	2
	4 × 10^{-8}–4 × 10^{-6}	4.27 × 10^{6}	0.99	200 pM	
	4 × 10^{-6}–5 × 10^{-5}	1.48 × 10^{5}	0.93	200 pM	
ClDNB	2 × 10^{-11}–2 × 10^{-8}	4.18 × 10^{8}	0.95	1 nM	10
	5 × 10^{-8}–5 × 10^{-5}	8.85 × 10^{4}	0.95	1 nM	

[a]LOD = lower limit of detection; max[x] = after addition of x equiv of NAC, only a residual change in FI is observed.

DOI: 10.1021/acsami.5b01970
ACS Appl. Mater. Interfaces 2015, 7, 10491−10500

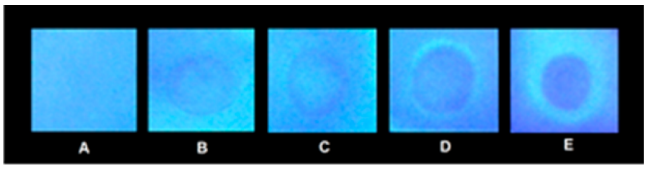

Figure 10. Photographs of fluorescence quenching (under 365 nm UV light) of paper strips coated with TRIPOD-TP and different amounts of PA: (A) drop of water; (B) 10^{-17}, (C) 10^{-15}, (D) 10^{-13}, and (E) 10^{-9} M. The size of each paper strip is 1.0 cm^2.

under 365 nm light illumination. For 10 μL of 10^{-17} M solution, this amounts to 60 molecules of PA.

To quantify PA using TRIPOD-TP-coated paper strips, we recorded the fluorescence spectra of the paper strips treated with different concentrations of PA. The plot of fluorescence intensity vs log [PA] shows a linear change and is in agreement with an exponential decrease in the fluorescence intensity (Figure 11) with the addition of PA as observed in the solution phase. The K_{sv} value, as determined by exponential equation $I/I_o = Ae^{Ksv[Q]} + B$, is found to be 2.48×10^{11} M^{-1} and is in close agreement with K_{sv} (1.20×10^{11} M) observed in the solution phase at low concentrations of PA. The addition of water did not quench the fluorescence intensity of the paper strip. Therefore, paper strips coated with TRIPOD-TP were highly sensitive to PA and could be used for quantification of 10^{-17}–10^{-6} M PA solutions.

CONCLUSION

In conclusion, we have synthesized a 1-(*p*-terphenyl)-benzimidazolium-based probe (TRIPOD-TP), which depending on the amount of PA added, can undergo a complex aggregation/disaggregation process. This was associated with amplified (>88%) fluorescence quenching to enable ultratrace detection of picric acid. FESEM and TEM studies along with DLS investigations provided deep insight into the aggregation/disaggregation process. In the solution phase, TRIPOD-TP could detect 5×10^{-13} M PA. Paper strips coated with TRIPOD-TP could detect as low as 10 μL of 10^{-17} M PA both qualitatively and quantitatively by the naked eye (under 365 nm lamp) through visible fluorescence quenching and upon measuring front surface steady state fluorescence, respectively. The other NACs, including 2,4-DNP, TNT, and ClDNB, also resulted in amplified fluorescence quenching but only at significantly higher concentrations. Therefore, the present study provides new insight into the design of self-assembled molecular probes for the detection of nitro-aromatic explosives.

EXPERIMENTAL SECTION

Materials and Reagents. All chemicals were obtained from common suppliers (Aldrich, SD Fine Chemicals Ltd., Spectrochem, etc.) and were used without further purification. Deionized water was obtained from ULTRA UV/UF Rions Lab Water System Ultra 370 series.

Instrumentation. ^{1}H and ^{13}C NMR spectra were recorded on BRUKER Bio spin AVANCE-III FT NMR HD-500 spectrophotometers using $CDCl_3$ or DMSO-d_6 as solvent and tetramethylsilane (TMS) as the internal standard. Data are reported as follows: chemical shifts in ppm, coupling constants (J) in Hz; and multiplicity as s = singlet, d = doublet, t = triplet, m = multiplet. High resolution mass spectra were recorded on a BRUKER DALTONIK micrOTOF-Q11 spectrometer. UV–vis studies of compounds were performed on a SHIMADZU-2450 spectrophotometer with a quartz cuvette of path length 1 cm. The cell holder was thermostated at 25.0 ± 0.2 °C. The fluorescence spectra were recorded on BH-CHRONOS fluorescence spectrophotometers with a quartz cuvette path length of 1 cm. The cell holder was thermostated at 25.0 ± 0.2 °C. The SEM images were obtained with a FESEM JEOL JSM-6610LV. The TEM images were obtained with a JEOL JEM-2100 electron microscope. DLS experiments were performed on a Malvern zetasizer. The time-resolved fluorescence spectra were recorded with a BH-CHRONOS time-resolved fluorescence spectrophotometer.

Quantum Yield Calculations.[58] Fluorescence quantum yields (Φs) were determined using an optically matched solution of QHS (Quin hydrogen sulfate) solution (Φs = 0.54 in 0.1 M H_2SO_4 solution) as the standard at an excitation wavelength of 290 nm, and quantum yield is calculated using the equation

$$\Phi_{fs} = \Phi_{fr}\frac{A_r}{A_s}\frac{n_s^2}{n_r^2}\frac{D_s}{D_r}$$

where Φ_{fs} and Φ_{fr} are the radiative quantum yields of the sample and reference, respectively, D_s and D_r are the areas of emission for the sample and reference, respectively, A_s and A_r are the absorbances of the sample and reference, respectively, and n_s and n_r are the refractive indices of the sample and reference solutions, respectively.

UV–Vis and Fluorescence Titrations. Stock solution of TRIPOD-TP (1 mM) was prepared in DMSO. For experiments with TRIPOD-TP, we took 3 mL of the solution that contained 15 μL of the TRIPOD-TP solution in DMSO, 60 μL of DMSO, and 2.94 mL of water in a cuvette. Typically, aliquots of freshly prepared standard solutions (10^{-1} M) of sodium salts (Na^+X^-), where X = CN^-, F^-, Cl^-, Br^-, I^-, ClO_4^-, NO_3^-, SO_4^{2-}, HSO_4^-, SCN^-, AcO^-, and $H_2PO_4^-$, in deionized Millipore water were used to record UV–vis and fluorescence spectra. The standard solutions (10^{-1} M) of NACs, phenol, 2-nitrophenol (2-NP), 4-nitrophenol (4-NP), 2,4-dinitrophe-

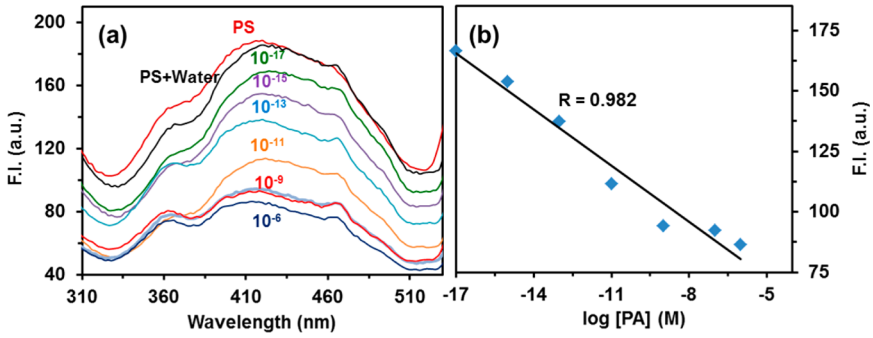

Figure 11. (a) Front surface steady-state fluorescence quenching of TRIPOD-TP with PA. PS = fluorescence spectrum of TRIPOD-TP-coated paper strip; PS + water = spectrum after addition of 200 μL of water to PS. 10^{-17}–10^{-6} corresponds to molar concentrations of PA added to PS. (b) Plot of fluorescence intensity of TRIPOD-TP vs log [PA] (M).

DOI: 10.1021/acsami.5b01970
ACS Appl. Mater. Interfaces 2015, 7, 10491–10500

nol (2,4-DNP), picric acid (PA), 4-hydroxybiphenyl (4-OHBP), 2-nitrotoluene (2-NT), 2,4-dinitrotoluene (2,4-DNT), dinitrobenzene (DNB), 2-chloronitrobenzene (2-ClNB), 2,4,6-trinitrotoluene (TNT), 3-chloronitrobenzene (3-ClNB), 4-chloro-nitrobenzene (4-ClNB), 1-chloro-2,4-dinitrobenzene (ClDNB), 2-nitroaniline (2-NA), and 2,4-dinitroaniline (2,4-DNA) were prepared in DMSO.

Detection Limit. The detection limit was calculated based on the fluorescence titration. To determine the S/N ratio, we measured the emission intensity of TRIPOD-TP (5 μM) without picric acid 5 times, and the standard deviation of blank measurements was determined. Under the present conditions, a good linear relationship between the fluorescence intensity and the picric acid concentration could be obtained between 5×10^{-13}–5×10^{-11} M ($R = 0.991$), 5×10^{-11}–5×10^{-8} M ($R = 0.981$), and 5×10^{-8}–1×10^{-6} M ($R = 0.997$) concentrations of PA for TRIPOD-TP. The detection limit is then calculated with the equation

$$\text{detection limit} = 3\sigma\text{bi}/m$$

where σbi is the standard deviation of blank measurements, and m is the slope between the intensity and sample concentration. The detection limit was measured to be 5×10^{-13} M at S/N = 3.

Synthesis of TRIPOD-TP. The solution of 1-(*p*-terphenyl)-benzimidazole (260 mg, 0.75 mmol) and 1,3,5-tris(bromo-methyl)-2,4,6-triethylbenzene (110 mg, 0.25 mmol) was heated in acetonitrile (15 mL) at 90 °C under N_2 for 24 h. The separated solid was filtered and washed with acetonitrile to obtain a white solid of TRIPOD-TP (335 mg); yield 90.5%; mp 245 °C; ^{1}H NMR (500 MHz, DMSO-d_6) δ 1.26 (bs, 9H, 3 × CH_3), 2.50 (bs, 6H, 3 × CH_2), 5.88 (s, 6H, 3 × CH_2), 7.34–7.40 (m, 9H, ArH), 7.52 (d, 6H, J = 6.5 Hz, ArH), 7.64 (s, 12H, ArH), 7.82 (t, 3H, J = 7.75 Hz, ArH), 7.90–7.94 (m, 18H, ArH), 8.56 (d, 3H, J = 8.5 Hz, ArH), 10.0 (s, 3H, Bim C2–H); ^{13}C NMR (125 MHz, DMSO-d_6) δ 16.0, 24.3, 45.7, 114.2, 114.7, 118.6, 126.8, 127.1, 127.7, 127.8, 128.1, 128.2, 128.4, 129.5, 132.0, 132.2, 132.6, 137.6, 139.3, 140.2, 141.7, 141.8, 149.0; HRMS-ESI calcd for $C_{90}H_{75}Br_3N_6$ m/z 659.2618, 660.2613 $[M - 2Br]^{2+}$, 413.2012 $[M - 3Br]^{3+}$, found 659.2890, 660.2897 $[M - 2Br]^{2+}$, 413.2190 $[M - 3Br]^{3+}$.

■ ASSOCIATED CONTENT

Supporting Information

General experimental information, UV and fluorescence spectra of TRIPOD-TP with increasing water ratios, ^{1}H NMR, ^{13}C NMR, and HRMS spectra of compound 1 and TRIPOD-TP, SAED, and XRD analysis of TRIPOD-TP (rods), DFT-optimized structure of TRIPOD-TP, SAED, and XRD analysis of TRIPOD-TP + PA (spherical aggregates), change in ^{1}H NMR spectrum of TRIPOD-TP upon addition of picric acid, and comparison of HOMOs and LUMOs of TRIPOD-TP and NACs. The Supporting Information is available free of charge on the ACS Publications website at DOI: 10.1021/acsami.5b01970.

■ AUTHOR INFORMATION

Corresponding Authors

*E-mail: prabhpreet1979@gmail.com.
*E-mail: subodh_gndu@yahoo.co.in.

Notes

The authors declare no competing financial interest.

■ ACKNOWLEDGMENTS

This work was supported by the Board of Research in Nuclear Science, Mumbai (2010/37C/6/BRNS/169) and the Department of Science and Technology, New Delhi (SR/S1/OC-75/2012). We thank UGC for the UPE program to the university, CAS status to the department, and DST for the FIST program. R.K. and S.S. acknowledge UGC and DST for fellowships.

■ ABBREVIATIONS

PA, picric acid
2,4-DNP, 2,4-dinitrophenol
TNT, 2,4,6-trinitrotoluene
ClDNB, 1-chloro-2,4-dinitrobenzene
TLC, thin-layer chromatography

■ REFERENCES

(1) Ownby, D.; Belden, J.; Lotufo, G.; Lydy, M. Accumulation of Trinitrotoluene (TNT) in Aquatic Organisms: Part 1-Bioconcentration and Distribution in Channel Catfish (*Ictalurus punctatus*). *Chemosphere* **2005**, *58*, 1153–1159.
(2) Lachance, B.; Robidoux, P.; Hawari, J.; Ampleman, G.; Thiboutot, S.; Sunahara, G. Cytotoxic and Genotoxic Effects of Energetic Compounds on Bacterial and Mammalian Cells in Vitro. *Mutat. Res., Genet. Toxicol. Environ. Mutagen.* **1999**, *444*, 25–39.
(3) Agrawal, J. P.; Hodgson, R. D. *Organic Chemistry of Explosives*; Wiley: Chichester, England, 2007.
(4) Singh, S. Sensors - An Effective Approach for the Detection of Explosives. *J. Hazard. Mater.* **2007**, *144*, 15–28.
(5) Smith, R. G.; DSouza, N.; Nicklin, S. A Review of Biosensors and Biologically-Inspired Systems for Explosives Detection. *Analyst (Cambridge, U.K.)* **2008**, *133*, 571–584.
(6) Steinfeld, J. I.; Wormhoudt, J. Explosives Detection: a Challenge for Physical Chemistry. *Annu. Rev. Phys. Chem.* **1998**, *49*, 203–232.
(7) Salinas, Y.; Martinez-Manez, R.; Marcos, M. D.; Sancenon, F.; Castero, A. M.; Parra, M.; Gil, S. Optical Chemosensors and Reagents to Detect Explosives. *Chem. Soc. Rev.* **2012**, *41*, 1261–1296.
(8) Germain, M. E.; Knapp, M. J. Optical Explosives Detection: from Color Changes to Fluorescence Turn-on. *Chem. Soc. Rev.* **2009**, *38*, 2543–2555.
(9) Venkatramaiah, N.; Kumar, S.; Patil, S. Fluoranthene based Fluorescent Chemosensors for Detection of Explosive Nitroaromatics. *Chem. Commun.* **2012**, *48*, 5007–5009.
(10) Kumar, S.; Venkatramaiah, N.; Patil, S. Fluoranthene based Derivatives for Detection of Trace Explosive Nitroaromatics. *J. Phys. Chem. C* **2013**, *117*, 7236–7245.
(11) Liang, Y.; Gu, L.; Liu, X.; Yang, Q.; Kajiura, H.; Li, Y.; Zhou, T.; Shi, G. Composites of Polyaniline Nanofibers and Molecularly Imprinted Polymers for Recognition of Nitroaromatic Compounds. *Chem.—Eur. J.* **2011**, *17*, 5989–5997.
(12) Xue, Y. S.; He, Y.; Zhou, L.; Chen, F. J.; Xu, Y.; Du, H. B.; You, X. Z.; Chen, B. A Photoluminescent Microporous Metal Organic Anionic Framework for Nitroaromatic Explosive Sensing. *J. Mater. Chem. A* **2013**, *1*, 4525–4530.
(13) Ma, Y.; Huang, S.; Deng, M.; Wang, L. White Upconversion Luminescence Nanocrystals for the Simultaneous and Selective Detection of 2,4,6-Trinitrotoluene and 2,4,6-Trinitrophenol. *ACS Appl. Mater. Interfaces* **2014**, *6*, 7790–7796.
(14) Chen, L.; Gao, Y.; Wang, Y.; He, C.; Zhu, D.; He, Q.; Cao, H.; Cheng, J. Femtogram Level Detection of Nitrate Ester Explosives via an 8-Pyrenyl-Substituted Fluorene Dimer Bridged by a 1,6-Hexanyl Unit. *ACS Appl. Mater. Interfaces* **2014**, *6*, 8817–8823.
(15) Mathew, A.; Sajanlal, P. R.; Pradeep, T. Selective Visual Detection of TNT at the Sub-Zeptomole Level. *Angew. Chem., Int. Ed.* **2012**, *51*, 9596–9600.
(16) Nagarkar, S. S.; Joarder, B.; Chaudhari, A. K.; Mukherjee, S.; Ghosh, S. K. Highly Selective Detection of Nitro Explosives by a Luminescent Metal–Organic Framework. *Angew. Chem., Int. Ed.* **2013**, *52*, 2881–2885.
(17) Mcquade, D. T.; Pullen, A. E.; Swager, T. M. Conjugated Polymer-Based Chemical Sensors. *Chem. Rev.* **2000**, *100*, 2537–2574.
(18) Thomas, S. W., III; Joly, G. D.; Swager, T. M. Chemical Sensors Based on Amplifying Fluorescent Conjugated Polymers. *Chem. Rev.* **2007**, *107*, 1339–1386.
(19) Rochat, S.; Swager, T. M. Conjugated Amplifying Polymers for Optical Sensing Applications. *ACS Appl. Mater. Interfaces* **2013**, *5*, 4488–4502.

DOI: 10.1021/acsami.5b01970
ACS Appl. Mater. Interfaces 2015, 7, 10491–10500

(20) Shu, W.; Guan, C.; Guo, W.; Wang, C.; Shen, Y. Conjugated Poly(aryleneethynylenesiloles) and their Application in Detecting Explosives. *J. Mater. Chem.* **2012**, *22*, 3075−3081.
(21) Sohn, H.; Sailor, M. J.; Magde, D.; Trogler, W. C. Detection of Nitroaromatic Explosives based on Photoluminescent Polymers Containing Metalloles. *J. Am. Chem. Soc.* **2003**, *125*, 3821−3830.
(22) Liu, J. Z.; Zhong, Y. C.; Lam, J. W. Y.; Lu, P.; Hong, Y. N.; Yu, Y.; Yue, Y. N.; Faisal, M.; Sung, H. H. Y.; Williams, I. D.; Wong, K. S.; Tang, B. Z. Hyperbranched Conjugated Polysiloles: Synthesis, Structure, Aggregation-enhanced Emission, Multicolor Fluorescent Photopatterning, and Superamplified Detection of Explosives. *Macromolecules* **2010**, *43*, 4921−4936.
(23) Yang, J.; Aschemeyer, S.; Martinez, H. P.; Trogler, W. C. Hollow Silica Nanospheres Containing a Silafluorene−Fluorene Conjugated Polymer for Aqueous TNT and RDX Detection. *Chem. Commun.* **2010**, *46*, 6804−6806.
(24) Toal, S. J.; Magde, D.; Trogler, W. C. Luminescent Oligo(tetraphenyl)silole Nanoparticles as Chemical Sensors for Aqueous TNT. *Chem. Commun.* **2005**, 5465−5467.
(25) Sohn, H.; Calhoun, R. M.; Sailor, M. J.; Trogler, W. C. Detection of TNT and Picric Acid on Surfaces and in Seawater by Using Photoluminescent Polysiloles. *Angew. Chem., Int. Ed.* **2001**, *40*, 2104−2105.
(26) Sanchez, J. C.; Urbas, S. A.; Toal, S. J.; DiPasquale, A. G.; Rheingold, A. L.; Trogler, W. C. Catalytic Hydrosilylation Routes to Divinylbenzene Bridged Silole and Silafluorene Polymers. Applications to Surface Imaging of Explosive Particulates. *Macromolecules* **2008**, *41*, 1237−1245.
(27) Rose, A.; Zhu, Z.; Madigan, C. F.; Swager, T. M.; Bulovi, V. Sensitivity Gains in Chemosensing by Lasing Action in Organic Polymers. *Nature* **2005**, *434*, 876−879.
(28) Zhao, D.; Swager, T. M. Sensory Responses in Solution vs Solid State: A Fluorescence Quenching Study of Poly(iptycenebutadiynylene)s. *Macromolecules* **2005**, *38*, 9377−9384.
(29) Yang, J. S.; Swager, T. M. Porous Shape Persistent Fluorescent Polymer Films: An Approach to TNT Sensory Materials. *J. Am. Chem. Soc.* **1998**, *120*, 5321−5322.
(30) Zahn, S.; Swager, T. M. Three-Dimensional Electronic Delocalization in Chiral Conjugated Polymers. *Angew. Chem., Int. Ed.* **2002**, *41*, 4225−4230.
(31) Yang, J. S.; Swager, T. M. Fluorescent Porous Polymer Films as TNT Chemosensors: Electronic and Structural Effects. *J. Am. Chem. Soc.* **1998**, *120*, 11864−11873.
(32) Swager, T. M. Iptycenes in the Design of High Performance Polymers. *Acc. Chem. Res.* **2008**, *41*, 1181−1189.
(33) Wang, Y.; La, A.; Ding, Y.; Liu, Y.; Lei, Y. Novel Signal-Amplifying Fluorescent Nanofibers for Naked-Eye based Ultrasensitive Detection of Buried Explosives and Explosive Vapors. *Adv. Funct. Mater.* **2012**, *22*, 3547−3555.
(34) Zhang, C.; Che, Y.; Yang, X.; Bunes, B. R.; Zang, L. Organic Nanofibrils based on Linear Carbazole Trimer for Explosive Sensing. *Chem. Commun.* **2010**, *46*, 5560−5562.
(35) Balakrishnan, K.; Datar, A.; Zhang, W.; Yang, X.; Naddo, T.; Huang, J.; Zuo, J.; Yen, M.; Moore, J. S.; Zang, L. Nanofibril Self-Assembly of an Arylene Ethynylene Macrocycle. *J. Am. Chem. Soc.* **2006**, *128*, 6576−6577.
(36) Naddo, T.; Che, Y.; Zhang, W.; Balakrishnan, K.; Yang, X.; Yen, M.; Zhao, J.; Moore, J. S.; Zang, L. Detection of Explosives with a Fluorescent Nanofibril Film. *J. Am. Chem. Soc.* **2007**, *129*, 6978−6979.
(37) Kartha, K. K.; Babu, S. S.; Srinivasan, S.; Ajayaghosh, A. Attogram Sensing of Trinitrotoluene with a Self-Assembled Molecular Gelator. *J. Am. Chem. Soc.* **2012**, *134*, 4834−4841.
(38) Bhalla, V.; Gupta, A.; Kumar, M.; Shankar Rao, D. S.; Prasad, S. K. Self-Assembled Pentacenequinone Derivative for Trace Detection of Picric Acid. *ACS Appl. Mater. Interfaces* **2013**, *5*, 672−679.
(39) Liao, Y. Z.; Strong, V.; Wang, Y.; Li, X.-G.; Wang, X.; Kaner, R. B. Oligotriphenylene Nanofiber Sensors for Detection of Nitro-Based Explosives. *Adv. Funct. Mater.* **2012**, *22*, 726−735.
(40) Anzenbacher, P., Jr.; Mosca, L.; Palacios, M. A.; Zyryanov, G. V.; Koutnik, P. Iptycene-Based Fluorescent Sensors for Nitroaromatics and TNT. *Chem.—Eur. J.* **2012**, *18*, 12712−12718.
(41) Barman, S.; Garg, J. A.; Blacque, O.; Venkatsen, K.; Berke, H. Triptycene based Luminescent Metal−Organic Gels for Chemosensing. *Chem. Commun.* **2012**, *48*, 11127−11129.
(42) Liu, T.; Ding, L.; Zhao, K.; Wang, W.; Fang, Y. Single-Layer Assembly of Pyrene End-capped Terthiophene and its Sensing Performances to Nitroaromatic Explosives. *J. Mater. Chem.* **2012**, *22*, 1069−1077.
(43) Feng, H.; Zheng, Y. Highly Sensitive and Selective Detection of Nitrophenolic Explosives by Using Nanospheres of a Tetraphenylethylene Macrocycle Displaying Aggregation-Induced Emission. *Chem.—Eur. J.* **2014**, *20*, 195−201.
(44) Peng, Y.; Zhang, A. J.; Dong, M.; Wang, Y. W. A Colorimetric and Fluorescent Chemosensor for the Detection of an Explosive - 2,4,6-Trinitrophenol (TNP). *Chem. Commun.* **2011**, *47*, 4505−4507.
(45) Kumar, R.; Sandhu, S.; Singh, P.; Hundal, G.; Hundal, M. S.; Kumar, S. Tripodal Fluorescent Sensor for Encapsulation-based Detection of Picric Acid in Water. *Asian J. Org. Chem.* **2014**, *3*, 805−813.
(46) Zhang, S.; Du, D.; Qin, J.; Bao, S.; Li, S.; He, W.; Lan, Y.; Shen, P. Z.; Su, A. Fluorescent Sensor for Highly Selective Detection of Nitroaromatic Explosives based on a 2D, Extremely Stable, Metal−Organic Framework. *Chem.—Eur. J.* **2014**, *20*, 3589−3594.
(47) Bhalla, V.; Arora, H.; Singh, H.; Kumar, M. Triphenylene Derivatives: Chemosensors for Sensitive Detection of Nitroaromatic Explosives. *Dalton Trans.* **2013**, *42*, 969−974.
(48) Das, S.; Chatterjee, D. P.; Samanta, S.; Nandi, A. K. Thermo and pH Responsive Water Soluble Polythiophene Graft Copolymer Showing Logic Operation and Nitroaromatic Sensing. *RSC Adv.* **2013**, *3*, 17540−17550.
(49) Wang, J.; Mei, J.; Yuan, W.; Lu, P.; Qin, A.; Sun, J.; Ma, Y.; Tang, B. Z. Hyperbranched Polytriazoles with High Molecular Compressibility: Aggregation-Induced Emission and Superamplified Explosive Detection. *J. Mater. Chem.* **2011**, *21*, 4056−4059.
(50) Samanta, D.; Mukherjee, P. S. Pt^{II}_6 Nanoscopic Cages with an Organometallic Backbone as Sensors for Picric Acid. *Dalton Trans.* **2013**, *42*, 16784−16795.
(51) Liu, J.-Z.; Zhong, Y.-C.; Lu, P.; Hong, Y.-N.; Lam, J. W. Y.; Faisal, M.; Yu, Y.; Wong, K. S.; Tang, B.-Z. A Superamplification Effect in the Detection of Explosives by a Fluorescent Hyperbranched Poly(silylenephenylene) with Aggregation-Enhanced Emission Characteristics. *Polym. Chem.* **2010**, *1*, 426−429.
(52) Zhang, L.; Zhao, C.; Zhou, J.; Kondo, T. Fluorescent Micelles based on Hydrophobically Modified Cationic Cellulose for Sensing Trace Explosives in Aqueous Solutions. *J. Mater. Chem. C* **2013**, *1*, 5756−5764.
(53) Mokac, J.; Bond, A. M.; Mitchell, S.; Scollary, G. A Statistical Overview of Standard (IUPAC and ACS) and New Procedures for Determining the limits of Detection and Quantification: Application to Voltammetric and Stripping Techniques (Technical Report). *Pure Appl. Chem.* **1997**, *69*, 297−328.
(54) Schröter, J. A.; Tschierske, C.; Wittenberg, M.; Wendorff, J. H. Liquid-Crystalline Crown Ether: Forming Columnar Mesophases by Molecular Recognition. *Angew. Chem., Int. Ed. Engl.* **1997**, *36*, 1119−1121.
(55) Liu, F.; Chen, B.; Glettner, B.; Prehm, M.; Das, M. K.; Baumeister, U.; Zeng, X.; Ungar, G.; Tschierske, C. The Trapezoidal Cylinder Phase: A New Mode of Self-Assembly in Liquid-Crystalline Soft Matter. *J. Am. Chem. Soc.* **2008**, *130* (30), 9666−9667.
(56) Cui, J.; Liu, A.; Guan, Y.; Zheng, J.; Shen, Z.; Wan, X. Tuning the Helicity of Self-Assembled Structure of a Sugar-based Organogelator by the Proper Choice of Cooling Rate. *Langmuir* **2010**, *26*, 3615−3622.
(57) Prehm, M.; Liu, F.; Zeng, X.; Ungar, G.; Tschierske, C. Axial-Bundle Phases − New Modes of 2D, 3D, and Helical Columnar Self-Assembly in Liquid Crystalline Phases of Bolaamphiphiles with Swallow Tail Lateral Chains. *J. Am. Chem. Soc.* **2011**, *133*, 4906−4916.

DOI: 10.1021/acsami.5b01970
ACS Appl. Mater. Interfaces 2015, 7, 10491−10500

(58) Demas, J. N.; Grosby, G. A. Measurement of Photoluminescence Quantum Yields. Review. *J. Phys. Chem.* **1971**, *75*, 991−1024.

DOI: 10.1021/acsami.5b01970
ACS Appl. Mater. Interfaces 2015, 7, 10491−10500